

A MULTI-WAVELENGTH STUDY OF THE γ -ray BINARY CANDIDATE HESS J1832-093

PAK-HIN THOMAS TAM¹, K. K. LEE², YUDONG CUI¹, A. K. H. KONG³, K. L. LI⁴, VLAD TUDOR⁵, XINBO HE¹, C. P. HU^{6,7},
 PARTHA S. PAL¹

¹ School of Physics and Astronomy, Sun Yat-sen University, Zhuhai 519082, China

² Department of Physics, The Chinese University of Hong Kong, Shatin, N.T., Hong Kong SAR, China

³ Institute of Astronomy, National Tsing Hua University 101, Section 2, Kuang-Fu Road, Hsinchu, 30013, Taiwan, R.O.C.

⁴ Department of Physics, UNIST, Ulsan 44919, Korea

⁵ International Centre for Radio Astronomy Research, Curtin University, GPO Box U1987, Perth, WA 6845, Australia

⁶ Department of Astronomy, Kyoto University, Kitashirakawa-Oiwake-cho, Sakyo-ku, Kyoto 606-8502, Japan

⁷ JSPS International Research Fellow

ABSTRACT

We investigate the nature of the unidentified very-high-energy (VHE) γ -ray object, HESS J1832-093, in a multi-wavelength context. Based on X-ray variability and spectral index ($\Gamma_X \sim 1.5$), and its broad-band spectrum (which **was** remarkably similar to HESS J0632+057, a confirmed γ -ray binary), HESS J1832-093 has been considered to be a strong γ -ray binary candidate **in previous works**. In this work, we provide further evidence for this scenario. We obtained a spectrum of its IR counterpart using Gemini/**Flamingo**, finding absorption lines that are usually seen in massive stars, in particular O stars. We also obtained a rather steep ATCA spectrum ($\alpha = -1.18^{+1.04}_{-0.88}$) which prefers a γ -ray binary over an AGN scenario. Based on spatial-spectral analysis and variability search, we found that 4FGL J1832.9-0913 is **possible to be associated with SNR G22.7-0.2 rather than with HESS J1832-093 only**.

Keywords: X rays: binaries — gamma rays: observations

1. INTRODUCTION

γ -ray binaries are a class of high-mass X-ray binaries which radiates dominantly in the γ -ray energy band in the νF_ν representation (Dubus 2013). Composing of a neutron star or a black hole, and a O/Be companion, γ -ray binaries consist of only **several well established members until 2019**: PSR B1259–63, LS I 61 303, LS 5039, HESS J0632-057, **1FGL J1018-5658** (Dubus 2015; Li et al. 2017a), PSR J2032+4127 (Lyne et al. 2015; Ho et al. 2017; Abeysekara et al. 2018), 4FGL J1405.1-6119 (Corbet et al. 2019), and a point source “P3” in the Large Magellanic Cloud (LMC) (Corbet et al. 2016; HESS Collaboration 2018). All of them have been detected above 100 GeV by ground-based Cherenkov telescopes **and/or** at 100 MeV to 100 GeV by the Large Area Telescope (LAT) onboard the *Fermi* satellite.

The Cherenkov telescope array, High Energy Stereoscopic System (H.E.S.S.), was used to discover HESS J1832–093 in the vicinity of SNR G22.7–0.2. It is seen as a point source by H.E.S.S., and its 0.4–5 TeV spectrum is well fit by a single power law with photon index of $\Gamma_{\text{TeV}} = 2.6 \pm 0.3_{\text{stat}} \pm 0.1_{\text{syst}}$. Its flux is around 1% that of the Crab nebula above 1 TeV. The observations were carried out from 2004 to 2011, comprising 67 hours live time, and no variability were found in the data (HESS Collaboration 2015). Based on its vicinity with SNR G22.7–0.2 and a spatially coincident CO emission, an SNR-molecular cloud interaction scenario was suggested. HESS Collaboration (2015) also used >10 GeV data from the *Fermi*/LAT and did not find any significant emission.

HESS J1832–093 has been observed with various X-ray instruments since 2008. An X-ray source, XMMU J183245–0921539, consistent with the location of HESS J1832–093, was found in a dedicated *XMM-Newton* observation in 2011 (HESS Collaboration 2015). While the X-ray column density of $N_H \sim 10^{23} \text{ cm}^{-2}$ toward the source is high (Eger et al. 2016; Mori et al. 2017), its X-ray emission is at the level of $10^{12} \text{ erg cm}^{-2} \text{ s}^{-1}$ with a hard photon index of ~ 1.5 . A *Chandra* observation in July 2015 (MJD 57209) was used to refine the *XMM-Newton* source location and it is fully consistent with an

Table 1. The r -value and equivalent widths (EWs) of each identified line feature.

Line	r	EW(\AA)
Br11 (1.6811 μm)	8.55	1.49 ± 0.44
Br γ (2.1661 μm)	7.48	3.75 ± 0.59
He I (1.7007 μm)	6.45	1.89 ± 0.39
He II (1.6923 μm)	4.59	1.68 ± 0.41
He II (2.189 μm)	4.13	1.44 ± 0.34

infrared (IR) source, 2MASS J18324516–0921545 (Eger *et al.* 2016). It is very likely that the IR, X-ray and TeV sources are associated with each other based on the spatial coincidence. The *Chandra* observation also constrained the X-ray source size to be <0.28 arcsec with 90% confidence. *NuSTAR* detects X-rays up to 30 keV with a $\Gamma_X = 1.5 \pm 0.1$ spectrum, showing particle acceleration typically seen in Galactic γ -ray binary systems. No X-ray periodicity from 4ms to 85.7 ks was found in the *NuSTAR* data (Mori *et al.* 2017).

Eger *et al.* (2016) reported that *Chandra* saw XMMU J183245–0921539 at an elevated X-ray flux state (on MJD 57209; about a factor of 6 above other measured X-ray flux), while the X-ray flux at other epochs (obtained by Swift/XRT and *XMM-Newton* observations) are consistent with being constant (Eger *et al.* 2016). However, this level of variability is disputed (Mori *et al.* 2017), who instead suggest an X-ray variability at the level of 50% based on the *XMM-Newton* and *NuSTAR* flux at two different epochs. If confirmed, such a variability almost certainly rules out scenarios that predict steady emission, including SNR-molecular cloud interaction or a putative pulsar wind nebula. Instead, as discussed in Eger *et al.* (2016), we seem to left with two scenarios: a γ -ray binary or an active galactic nucleus (AGN).

There is no known optical counterpart, and it is likely because of high level of absorption revealed by the X-ray data. Spitzer detected the IR counterpart, 2MASS J18324516–0921545, up to 8 μm (from the catalogue; source name SSTGLMC G022.4768-00.1539). Pan-STARRS have a few measurements in the z ($=20.32 \pm 0.135$) and y ($=19.702 \pm 0.05$) bands.

To further probe the origin of HESS J1832–093, we obtained Gemini-south NIR spectroscopic observations and investigate the *Fermi*-LAT data obtained over the first 10.6 years. We also obtained data by ATCA (2016 June 2) and Swift/XRT (up to MJD 58287). Based on the multi-wavelength datasets, we argue that HESS J1832–093 is indeed a γ -ray binary.

2. GEMINI NEAR-INFRARED OBSERVATION

We obtained a Fast Turnaround (FT) mode of observation using the FLAMINGOS-2 (long-slit spectrograph) instrument at the Gemini-south Observatory on June 2, 2016. The data reduction was done using the IRAF¹ software. The spectra that we obtained are shown in the upper panel of Fig. 1. The data quality is not particularly high and we note several strong telluric absorption lines due to water vapor.

To quantify the signal-to-noise ratio of any stellar lines among the telluric lines, we define r to be (Area of the absorption lines measured - Area of the telluric absorption lines)/(Area of the telluric absorption lines), and identify four lines with $r > 4$, which are shown in Table 1, together with their equivalent widths. The region longer than 1.72 μm in H-band is severely contaminated, and the contamination is more severe in H-band than in K-band. To make the situation more explicit, we depict in the bottom panel of Fig. 1 the IR transmission spectra taken from the Gemini website².

We found evidence of the lines related to Br γ , Br11, He I, and He II, many of which are seen in massive stars only:

1. The HeII 2.189 μm line is seen in O stars but not B stars (Martins *et al.* 2019);
2. He II (1.6923 μm) line appears only in the O-type star (Hanson *et al.* 1998; Roman-Lopes *et al.* 2018);
3. The equivalent width of He I (1.7007 μm) line shows that the spectral type should be before O8 or after B2 (Blum *et al.* 1997);

¹ IRAF is distributed by the National Optical Astronomy Observatories.

² <https://www.gemini.edu/sciops/telescopes-and-sites/observing-condition-constraints/ir-transmission-spectra>

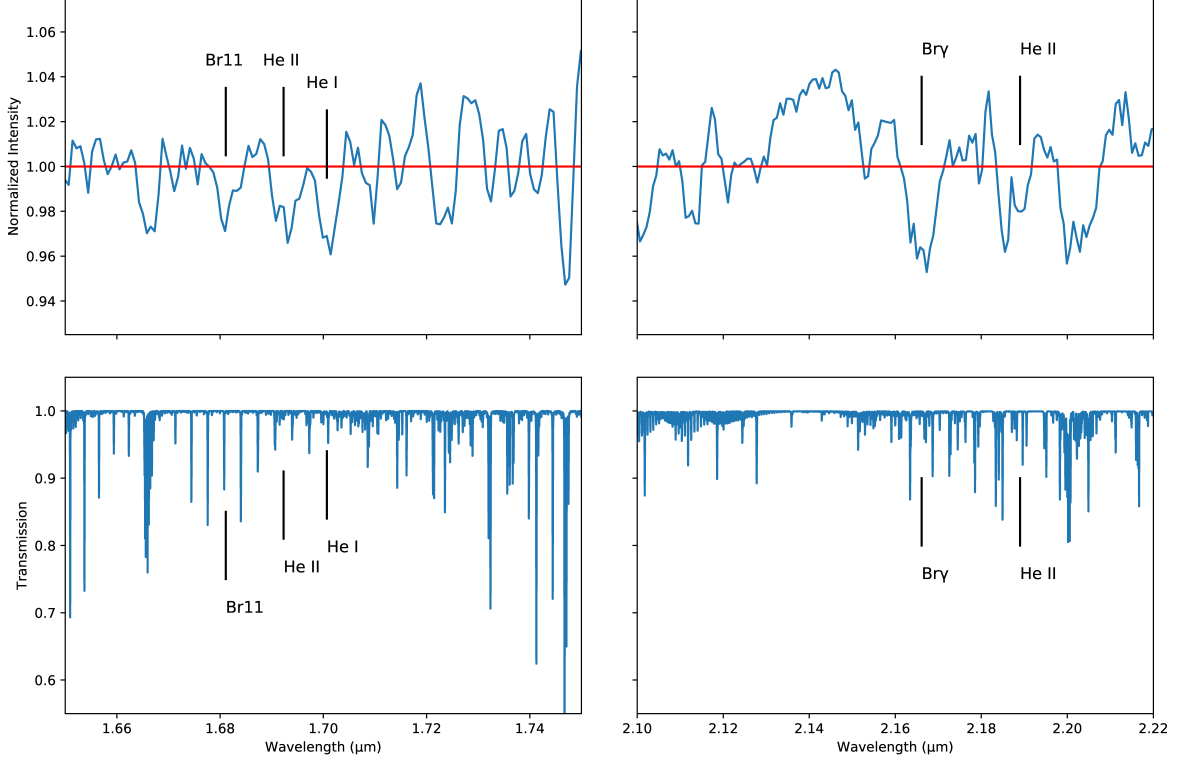


Figure 1. *Top panel:* The H-band (left) and K-band (right) spectrum taken with FLAMINGOS-2 at the Gemini-south Observatory on June 2, 2016. *Bottom panel:* the IR transmission spectra taken from the Gemini website.

4. The equivalent width of Br11 ($1.6811\mu\text{m}$) line would indicate that the star is an O-B1 star (Roman-Lopes *et al.* 2018).

Therefore, combining all the information above, we suggest that the IR counterpart of XMMU J183245–0921539 to be an O- or, less likely, early B-type star. The lack of prominent emission line in NIR also rules out a circumstellar disk normally associated with a Be star. Therefore, we conclude that the NIR counterpart is a massive star, and not an AGN. This conclusion is consistent with the photometric considerations (in J- and K-band) reported in Mori *et al.* (2017).

3. *FERMI*/LAT OBSERVATIONS OF HESS J1832–093

The LAT detector is an all-sky monitor at energies from several tens of MeV to more than 300 GeV (Atwood *et al.* 2009). The γ -ray data³ used in this work were obtained using the *Fermi*/LAT between 2008 August 4 and 2019 March 13. We used *Fermi*tools 1.0.0 to reduce and analyze the data. Pass 8 data with energy 100 MeV to 500 GeV classified as “source” events were used. To reduce the contamination from Earth albedo γ -rays, events with zenith angles greater than 90° were excluded. The instrument response functions “P8R3_SOURCE_V2” were used.

3.1. *Maximum Likelihood Analysis*

We carried out a binned maximum-likelihood analysis (*gtlike*) of a rectangular region of $15^\circ \times 15^\circ$ centered on the position of HESS J1832–093. We subtracted the background contribution by including the Galactic diffuse model (gll_iem_v07.fits) and the isotropic background (iso_P8R3_SOURCE_V2_v1.txt) as well as the 4FGL (Abdollahi *et al.* 2019) sources within 20° away from HESS J1832–093. FL8Y⁴ sources were also employed (instead of 4FGL sources) for cross-check purpose. In the FL8Y/4FGL catalog, one source, 4FGL J1832.9-0913 (i.e., FL8Y J1832.5-0921), is said to be associated with HESS J1832-093/SNR G022.7-0.2, in accordance to HESS Collaboration (2015). Moreover, both catalog sources locate very close to HESS J1832–093, hence we did not treat FL8Y J1832.5-0921/4FGL J1832.9-0913 as a background source in our analysis. The γ -ray pulsars PSR J1831-0952 and PSR J1833-1034 are within one degree

³ provided by the FSSC at <http://Fermi.gsfc.nasa.gov/ssc/>

⁴ <https://Fermi.gsfc.nasa.gov/ssc/data/access/lat/fl8y/>

from HESS J1832–093. The former γ -ray pulsar was reported in [Laffon et al. \(2015\)](#) and no timing ephemeris has been given. Considering also that the current available timing ephemeris of the latter is valid until 2013 October only, c.f. http://www.slac.stanford.edu/~kerrm/Fermi_pulsar_timing/, we did not perform pulsar gating in the likelihood analysis. We, however, include 4FGL J1831.5-0935 (associated with PSR J1831-0952) in the background model as this pulsar is within 0.4 degree from HESS J1832–093. The recommended spectral model for each source as in the corresponding catalog was used, while we modeled a putative source exactly at the position of HESS J1832–093 with a power law (PL)

$$\frac{dN}{dE} = N_0 \left(\frac{E}{E_0} \right)^{-\Gamma}, \quad (1)$$

where the normalization N_0 and spectral index Γ were allowed to vary. The normalization parameter values for the Galactic and isotropic diffuse components, and for the sources within 6° from HESS J1832–093, the normalization N_0 and spectral index Γ were allowed to vary as well.

HESS J1832–093 was detected with TS=95.8 in this analysis. The best-fit power-law index is 2.46 ± 0.70 , and the photon flux is $(5.10 \pm 1.48) \times 10^{-8}$ photons $\text{cm}^{-2} \text{s}^{-1}$. We repeated the analysis using photons within narrower energy bands (i.e., 0.1-0.3 GeV, 0.3-1.0 GeV, 1-3 GeV, 3-15 GeV, and 15-300 GeV), and the flux obtained is plotted in the spectral energy distribution (see Fig. 5). We also attempted to use a power-law with exponential cutoff (PLE), **and the best fit of PLE gives a spectral index of $\Gamma = 1.58 \pm 0.29$ and a cutoff energy of $E_c = 650 \pm 140$ MeV. However, PLE shows no statistical improvement.** To produce the TS map shown in Fig. 2, we use 1–500 GeV clean, front-converted photons to avoid low-energy photon contamination from nearby sources.

As the SNR G22.7-0.2 is only $11.5'$ from XMMU J183245–0921539, and the former can potentially contribute to or even dominate the γ -rays that we see (e.g., by SNR-molecular cloud interaction), we proceeded to add a hypothetical point source at the center of the SNR (since there is no a-priori knowledge about which molecular clouds the SNR may be interacting) and performed the maximum-likelihood analysis again. Comparing the three models (HESS J1832–093 only, G22.7-0.2 only, and both HESS J1832–093 and G22.7-0.2), the value of $-\log(\text{likelihood})$ is the lowest with both sources added (-38552671.38), suggesting that one source among the two dominate the γ -ray emission. The value of $-\log(\text{likelihood})$ is comparable for fits using HESS J1832–093 only (-38552668.78) or G22.7-0.2 only (-38552670.5). Therefore there is no strong preference as for which source (HESS J1832–093 versus G22.7-0.2) is the dominant GeV-emitting source (in other words, to be associated with 4FGL J1832.9-0913) based on this comparison only.

The exact position of 4FGL J1832.9-0913 can be estimated by the pixel in the TS map with the highest TS values, which is R.A.= $18^{\text{h}}33^{\text{m}}02^{\text{s}}.04$, Decl.= $-09^\circ13'43''.3$ (J2000).

Another test to help distinguish whether 4FGL J1832.9-0913 originates from HESS J1832–093 or G22.7-0.2, is to check the possible spatial extension of the source. For this purpose, we insert uniform disks of various radius, from 0.05° to 0.45° , centered on the TS peak position shown above. In this analysis, we used spatial bins of 0.02° to increase spatial resolution, while allowed the spectral parameters of sources within 3° from HESS J1832–093 to vary. Fig. 3 shows how the TS value of the source varies with increasing radius (which is an indicator of the possible extension). It can be seen that the highest TS value occur for a radius of 0.2° (or $12'$), and may suggest possible extension for 4FGL J1832.9-0913.

3.2. Periodicity and Variability Search

One distinguishing feature of γ -ray binaries are their orbital periodicity. We tried box-fitting algorithm ([Kovács et al. 2002](#)) and did not find any significant periodicity for time scales from 10^{-1} s to 10^3 s. We also created a γ -ray light curve using a bin size of 1 day and search for periodicity with Lomb-Scargle algorithm ([Lomb 1976](#); [Scargle 1982](#)). We further use REDFIT algorithm to estimate the red noise level ([Schulz & Mudelsee 2002](#)). Only a peak located at ~ 53.4 day, which is the precession period of the *Fermi* orbit, is clearly above the red noise level.

To probe any possible variability in GeV γ -rays, we produced light curves using the likelihood analysis for time bins of sizes 173.5 days, which is a balance between small photon statistics and the desire to probe variability on time scales shorter than about a year. The background source model used in the previous section is also used here. We do not see any significant change in flux nor spectral index in different time bins. A 88 day-binned light curve is also produced and again no strong variability can be seen.

To formally assess whether HESS J1832–093 varies at GeV energies, we follow the same treatment for variability as in 2FGL ([Nolan et al. 2012](#)), as well as in the 3FGL ([Acero et al. 2015](#)) catalog, by comparing the difference of the likelihood in the null hypothesis (the flux of HESS J1832–093 is stable over the full time range) and that in the

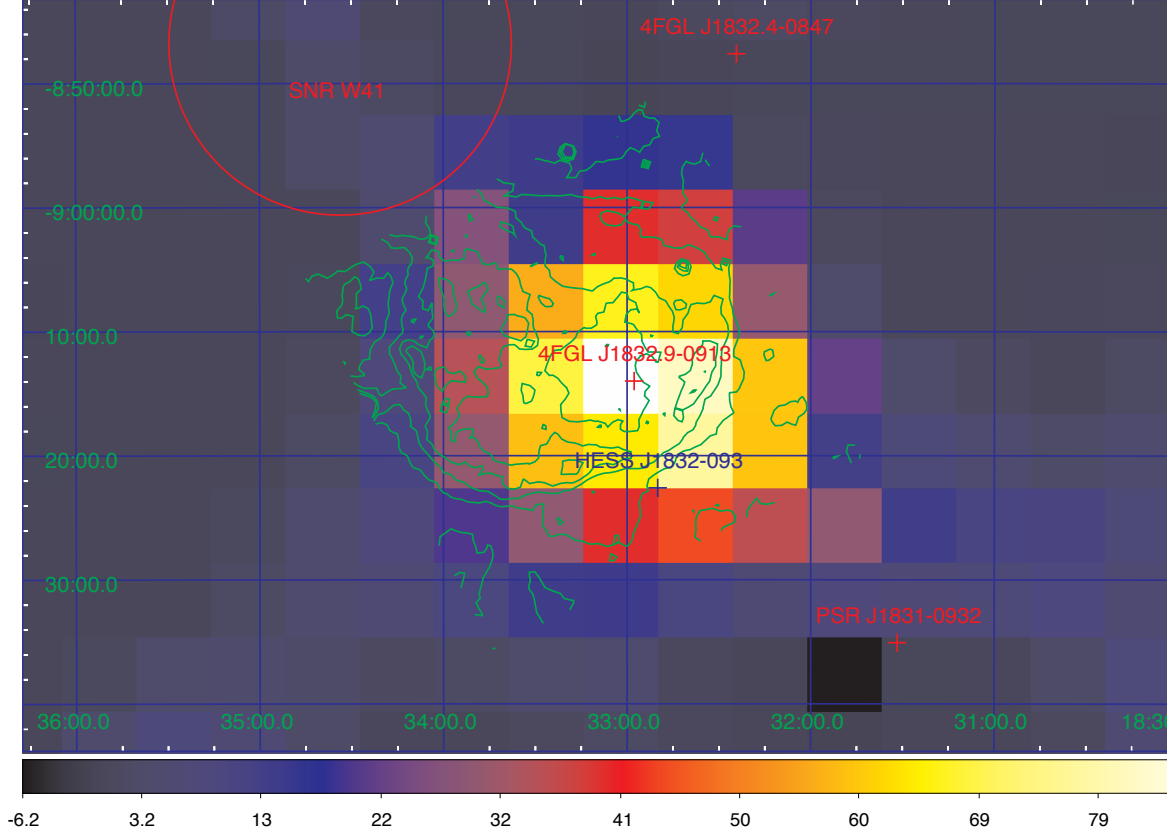


Figure 2. TS map of the $1 \text{ deg} \times 1 \text{ deg}$ region around 4FGL J1832.9-0913, using 1–500 GeV photons, overlaid in green contours is the 20 cm emission of G022.7-0.2 (from the Multi-Array Galactic Plane Imaging Survey, [White et al. 2005](#); [Helfand et al. 2006](#)). The x- and y-axis shows the R.A. and Decl., respectively.

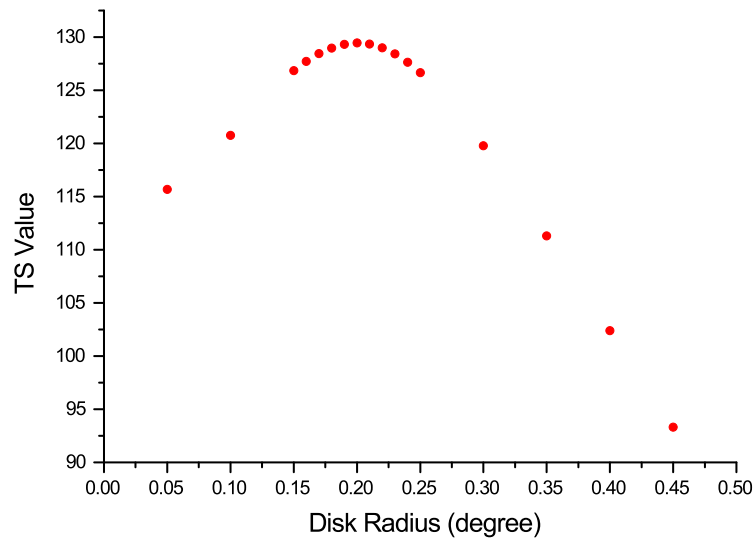


Figure 3. TS value of 4FGL J1832.9-0913 modeled with uniform disks of various radii

alternative hypothesis (the source flux is allowed to vary). The variability index thus obtained is 26.9, which for 21 degrees of freedom corresponds to a variability confidence level just below 90% (which would have a variability index 29.6). Therefore, we do not detect any significant variability.

4. ATCA RADIO OBSERVATIONS

We conducted radio continuum observations with ATCA under project CX359, when the array was in 1.5B configuration. These were carried out on 2 June 2016, 14:56 to 19:04 UT, for a total of 3.6h on-source. The Director’s discretionary Time (DDT) observations were prompted by the large X-ray flux variability reported by [Eger et al. \(2016\)](#). We simultaneously observed two frequency windows, centred at 5.5 and 9 GHz, each with a bandwidth of 2 GHz. We used the source PKS 1934-638 as a bandpass and flux calibrator, and 1829-106 as a phase calibrator.

The data were flagged and calibrated in Miriad v1.5 ([Sault et al. 1995](#)) using standard procedures. We imaged the data in CASA 4.5 ([McMullin et al. 2007](#)) using Briggs weighting of robustness 1, which balances sensitivity and spatial resolution.

Resolutions of $44.7'' \times 1.5''$ at 5.5 GHz and $25.7'' \times 1.2''$ at 9 GHz were achieved. We detected significant unresolved emission near the X-ray position of HESS J1832-093, which we characterised by fitting a point source in the image plane using the CASA IMFIT task. In the higher signal-to-noise image (5.5 GHz), the position of this source was RA (J2000) = $18:32:45.154 \pm (0.009\text{s or } 0.13'')$, DEC (J2000) = $-09:21:57.6 \pm 2.6''$, which is fully consistent with the *Chandra* position ([Eger et al. 2016](#)). At 5.5 GHz, we obtained the flux density of $S_{5.5} = 211 \pm 31 \mu\text{Jy}$. At 9 GHz, $S_9 = 118 \pm 37 \mu\text{Jy}$. Taking the conventional form of the spectral index α as in $S_\nu \sim \nu^\alpha$, one obtains $\alpha = -1.18^{+1.04}_{-0.88}$.

The steep spectrum does not suggest the radio source to be an AGN which should have a rather flat spectrum. Within the γ -ray binary scenario, this radio counterpart may be due to the synchrotron radiation from shocked electrons or a putative radio pulsar.

5. SWIFT/XRT OBSERVATIONS OF HESS J1832-093

Long-term X-ray monitoring is essential to check for any flare-like emission or variability of the source in X-rays. [Eger et al. \(2016\)](#) reported X-ray observations up to MJD 57291. We obtained 41 additional measurements from MJD 57460 to MJD 58287. The exposures ranges from < 1 ksec to 5 ksec. Most of them are useful to build a long-term X-ray light curve, but the data qualities are not good enough for meaningful spectral analyses. In particular, the photon index (Γ_X) and column density (N_H) is not constrained by the Swift data, therefore we take the value of N_H to be $9.5 \times 10^{22} \text{ cm}^{-2}$ and $\Gamma_X = 1.5$ which is obtained from a joint fit of the *Chandra*, *XMM-Newton*, and *NuSTAR* spectra ([Mori et al. 2017](#)). This gives a count-to-energy flux ratio of one count to $1.382 \times 10^{-10} \text{ ergs cm}^{-2} \text{ s}^{-1}$ (2–10 keV).

To extract the XRT light curve, we used the *Swift* online analysis tool⁵ ([Evans et al. 2007, 2009](#)) to take a good care of bad pixels, vignetting, and point spread function (PSF) corrections of the data. All parameters were left at program default values with the option *binning by observation* chosen.

The light curve (Fig. 4, beyond MJD 57200) is shown together with the *Chandra* and *NuSTAR* data as presented in [Mori et al. \(2017\)](#). Fitting the full XRT count rate (including those before MJD 57200) with a constant flux returns a $\chi^2(\text{d.o.f.})$ value of 38.5(40). Therefore, no significant variability can be inferred solely from the Swift/XRT data due primarily to the large error bars. We also attempted to search for periodicity at time scales > 0.5 day. No significant signal is seen, which again is subject to the low count rate and/or insufficient sampling seen by Swift/XRT.

6. DISCUSSION

Among the five firmly identified TeV γ -ray binaries so far, PSR B1259-63, LS 5039, LS I+61 303, and 1FGL J1018.6-5856 all exhibit a peak in their SED at MeV-GeV energies, while HESS J0632+057 may also have been detected in this energy band ([Li et al. 2017a](#)). A MeV-GeV peak may be due to synchrotron emission, see e.g. PSR B1259-63 by [Abdo et al. \(2011\)](#); [Tam et al. \(2015\)](#). For HESS J0632+057, with its SED peak possibly in TeV, an inverse-Compton (IC) dominated model has been considered ([Hinton et al. 2009](#); [Yi & Cheng 2017](#); [Barkov & Bosch-Ramon 2018](#)).

Based on our *Fermi* analysis results shown in Fig. 5, **the SED, i.e. the GeV band, of HESS J1832-093 looks like neither the ones of former four binaries, nor the one of HESS J0632+057.** Assuming the GeV emission is indeed due to HESS J1832-093, it would suggest that HESS J1832-093 is spectrally different from those previous identified

⁵ http://www.swift.ac.uk/user_objects/

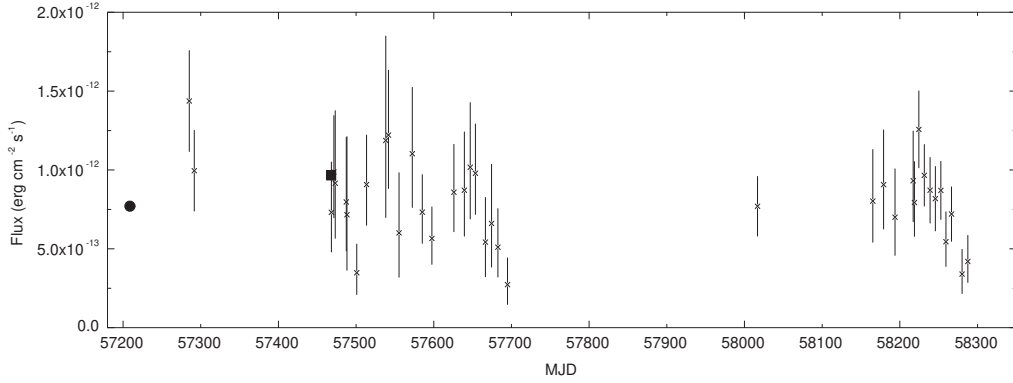


Figure 4. X-ray (2–10 keV) light curve (beyond MJD 57200) of HESS J1832–093 obtained using Swift/XRT(asterisk), *Chandra* (circle), and *NuSTAR* (square).

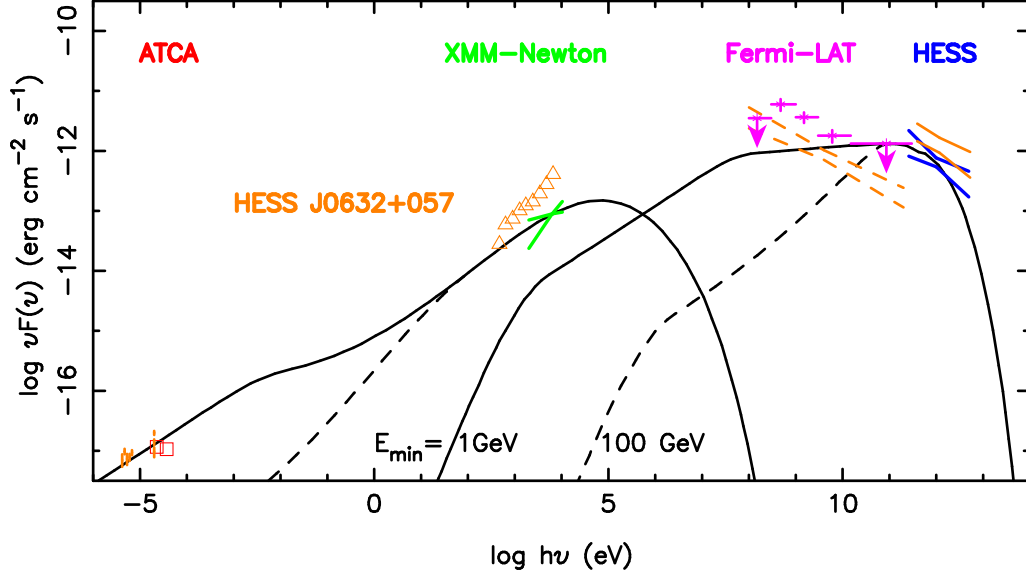


Figure 5. The SED of HESS J1832–093 and the IC-dominated model used in [Hinton et al. \(2009\)](#) and [Eger et al. \(2016\)](#). The data points of HESS J0632+057 ([Skilton et al. 2009](#)) is also shown in orange for comparison. The dashed line is the *Fermi* spectrum of Fermi J0632.6+0548, thought to be associated with HESS J0632+057 ([Li et al. 2017a](#)).

TeV γ -ray binaries. We test two simplified one-zone models to explain its SED, a synchrotron-dominated model (not shown) and a IC-dominated model (shown as in Fig. 5), both of which face difficulties to explain the spectrum of 4FGL J1832.9-0913. Adding alternative sources can help explaining the GeV spectrum, and the SNR G22.7-0.2 can very well be such an alternative source. As discussed in Section. 3.1, the possible extended morphology of 4FGL J1832.9-0913 also support this theory of alternative sources. If it is the case, the rather low break energy (~ 650 MeV in the PLE fit, see Sect. 3.1) is similar to the cases of middle-aged SNRs, e.g., W44 ([Abdo et al. 2012](#)) and W51C ([Abdo et al. 2009](#)). Future planned missions including *eastrogam* ([De Angelis et al. 2017](#)) and AMEGO ⁶, with their better PSF below 1 GeV, will certainly help.

7. CONCLUSION

⁶ <https://asd.gsfc.nasa.gov/amego/>

The X-ray and TeV spectrum of HESS J1832–093 is similar to other γ -ray binaries, e.g., HESS J0632+057, as noted before, suggesting HESS J1832–093 is also a γ -ray binary. In this work, we present **several additional observations to further explore this scenario**:

- We present the first NIR spectroscopy of the IR counterpart of HESS J1832–093, which identifies it as an O-, or less likely, early B-type star; this result is consistent with a photometric measurement (Mori et al. 2017);
- The rather steep ATCA spectrum does not suggest a radio AGN nature, and within the γ -ray binary scenario, such a spectrum may be consistent with the synchrotron radiation from shocked electrons or a radio pulsar residing in the binary. Further radio observations with more accurate spectral measurements and dedicated radio pulsar timing search are needed to confirm the latter scenario.
- **The GeV source – 4FGL J1832.9-0913 is located just $\sim 10'$ from HESS J1832–093, and well within the radio emission of the SNR G22.7-0.2. There is no significant evidence for variability of this source. Evidence of extension at a radius of $12'$ and the unique GeV spectrum which is difficult to be explained by conventional γ -ray binary models seem to support the SNR scenario.** In this case, HESS J1832–093 remains one of the only γ -ray binaries (candidates) without Fermi-LAT counterpart. Future missions with better PSF will certainly help for further verification of the nature of 4FGL J1832.9-0913.
- Mori et al. (2017) found a $\sim 50\%$ X-ray flux variability based on the *XMM-Newton* and *NuSTAR* observations. However, no significant variability can be inferred from the Swift/XRT data due primarily to the large error bars. This indicates that regular monitoring using sensitive X-ray instruments are needed to constrain the real X-ray light curve. Such a light curve is a possible way to identify the orbital period of HESS J1832–093, as the case for HESS J0632+057.

Ultimately, we find that the radio, IR, X-ray, and TeV point sources are associated with each other based on positional coincidence and they all support this γ -ray binary hypothesis, while 4FGL J1832.9-0913 is probably due to alternative sources, i.e., SNR G22.7-0.2.

This research made use of data supplied by the High Energy Astrophysics Science Archive Research Center (HEASARC) at NASA’s Goddard Space Flight Center, and the UK Swift Science Data Centre at the University of Leicester. We thank ATNF for the rapid scheduling of the ATCA observations. The Australia Telescope Compact Array is part of the Australia Telescope National Facility which is funded by the Australian Government for operation as a National Facility managed by CSIRO. This work is supported by the National Natural Science Foundation of China (NSFC) through grants 11633007, 11661161010, and U1731136.

REFERENCES

- Abdo, A. A., Ackermann, M., Ajello, M., et al. 2009, ApJL, 706, L1
- Abdo, A. A., Ackermann, M., Ajello, M., et al. 2011, ApJL, 736, L11
- Uchiyama, Y., Funk, S., Katagiri, H., et al. 2012, ApJL, 749, L35
- Abdollahi, S., Acero, F., Ackermann, M., et al. 2019, preprint[https://arxiv.org/abs/1902.10045]
- Abeysekara, A. U., Benbow, W., Bird, R., et al. 2018, ApJL, 867, L19
- Acero, F., Ackermann, M., Ajello, M., et al. 2015, ApJS, 218, 23
- Atwood, W. B., Abdo, A. A., Ackermann, M., et al. 2009, ApJ, 697, 1071
- Barkov, M. V. & Bosch-Ramon, V. 2018, MNRAS, 479, 1320
- Blum R. D., Ramond T. M., Conti P. S., Figer D. F., & Sellgren K., 1997, AJ, 113, 1855
- Clark J. S. & Steele I. A., 2000, AAS, 141, 65
- Corbet, R. H. D., Chomiuk, L., Coe, M. J., et al. 2016, ApJ, 829, 105
- De Angelis, A., Tatischeff, V., Grenier, I. A., et al. 2017, Journal of High Energy Astrophysics, 2018, 19, 1
- Dubus, G. 2013, A&A Rev., 21, 64
- Dubus, G. 2015, Comptes Rendus Physique, 16, 661
- Dubus, G., Guillard, N., Petrucci, P.-O., & Martin, P. 2017, A&A, 608, A59
- Eger, P., Laffon, H., Bordas, P., de Oña Whihelmi, E., Hinton, J., & Pühlhofer, G. 2016, MNRAS, 457, 1753
- Evans, P. A., Beardmore, A. P., Page, K. L., et al. 2007, A&A, 469, 379
- Evans, P. A., Beardmore, A. P., Page, K. L., et al. 2009, MNRAS, 397, 1177
- Corbet, R. H. D., Chomiuk, L., Coe, M. J., et al. 2019, ApJ, 884, 93
- Hanson, M. M., Rieke, G. H., & Luhman, K. L. 1998, AJ, 116, 1915
- Helfand, D. J., Becker, R. H., White, R. L., Fallon, A., & Tuttle, S. 2006, AJ, 131, 2525
- HESS Collaboration 2015, MNRAS, 446, 1163
- HESS Collaboration, Abdalla, H., Abramowski, A., et al. 2018, A&A, 610, L17
- Hinton, J. A., Skilton, J. L., Funk, S., et al. 2009, ApJL, 690, L101

- Ho, W. C. G., Ng, C.-Y., Lyne, A. G., et al. 2017, *MNRAS*, 464, 1211
- Kovács, G., Zucker, S., & Mazeh, T. 2002, *A&A*, 391, 369
- Laffon, H., Smith, D. A., Guillemot, L., & for the *Fermi*-LAT Collaboration 2015, 2014 *Fermi* Symposium proceedings - eConf C141020.1, preprint[arXiv:1502.03251]
- Li, J., Torres, D. F., Cheng, K.-S., et al. 2017a, *ApJ*, 846, 169
- Li, K. L., Kong, A. K. H., Tam, P. H. T., et al. 2017b, *ApJ*, 843, 85
- Li, K. L., Takata, J., Ng, C. W., et al. 2018, *ApJ*, 857, 123
- Lomb, N. R. 1982, *Astrophys. & Sp. Sci.*, 39, 447
- Lyne, A. G., Stappers, B. W., Keith, M. J., et al. 2015, *MNRAS*, 451, 581
- Martins, F., Chené, A.-N., Bouret, J.-C., Borissova, J., Groh, J., Ramírez Alegría, S., & Minniti, D. 2019, *A&A*, 627, A170
- McMullin, J. P., Waters, B., Schiebel, D., Young, W., & Golap, K. 2007, *Astronomical Data Analysis Software and Systems XVI*, 376, 127
- Mori, K., Gotthelf, E. V., Hailey, C. J., et al. 2017, *ApJ*, 848, 80
- Moritani, Y., Kawano, T., Chimasu, S., et al. 2018, *PASJ*, 70, 61
- Nolan, P. L., Abdo, A. A., Ackermann, M., et al. 2012, *ApJS*, 199, 31
- Roman-Lopes A., Román-Zúñiga C., Tapia Mauricio, et al. 2018, *AJ*, 885, 11
- Sault, R. J., Teuben, P. J., & Wright, M. C. H. 1995, *Astronomical Data Analysis Software and Systems IV*, 77, 433
- scargle82 Scargle, J. D. 1982, *ApJ*, 263, 835
- Schulz M., & Mudelsee, M. 2002, *Computers & Geosciences*, 28, 421
- Skilton, J. L., Pandey-Pommier, M., Hinton, J. A., et al. 2009, *MNRAS*, 399, 317
- Su, Y., Yang, J., Zhou, X., Zhou, P., & Chen, Y. 2014, *ApJ*, 796, 122
- Takata, J., Tam, P. H. T., Ng, C. W., et al. 2017, *ApJ*, 836, 241
- Tam, P. H. T., Li, K. L., Takata, J., et al. 2015, *ApJL*, 798, L26
- White, R. L., Becker, R. H., & Helfand, D. J. 2005, *AJ*, 130, 586
- Yi, S.-X. & Cheng, K. S. 2017, *MNRAS*, 471, 4228